Penerbit Akademia Baru

Journal of Advanced Research in Fluid Mechanics and Thermal Sciences
ISSN (online): 2289-7879 | Vol. 10, No. 1. Pages 11-26, 2015

Numerical Study on the Effect of Inclination Angles on Natural Convection in Entrance Region using Regularised Lattice Boltzmann BGK Method

*M. Basha and C. S. Nor Azwadi**

Department of Thermo-fluids, Faculty of Mechanical Engineering, Universiti Teknologi Malaysia, 81310 Johor, Malaysia.

**azwadi@fkm.utm.my*

Abstract – *A numerical study of incompressible laminar natural convection in entrance region of two dimensional vertical and inclined channels using Regularized Lattice Boltzmann Bhatnaghar-Gross-Krook (RLBGK) method is presented in this paper. Individual distribution functions with lattice types D2Q9 and D2Q5 are considered to solve fluid flow and thermal fields, respectively. Rayleigh number is varied from 10^2 to 10^6. The channel inclination angle is varied from 0 to 60°. Aspect ratio of channel is equal to 5. A set of distribution functions is proposed to mimic Bernoulli's equation for calculating pressure at the inlet. Predicted velocity and temperature fields are compared with velocity and temperature fields found from finite volume code Fluent. Also, predicted Nusselt numbers are compared with Nusselt numbers correlation. Results are in good agreement with results found from FLUENT code.*

Keywords: Lattice Boltzmann Method, Multi-Population Distribution, Natural Convection, Entrance Region, Channel

1.0 INTRODUCTION

Natural convection is one of the frequently observed heat transfer mechanism in electronic cooling. Natural convection in parallel plates or channel can be regarded as a basic module of physical heat transfer surface geometry of most of electronic components. Consequently, study on natural convection in channels has gained greater attention [1,2]. Traditionally, numerical methods such as finite difference, finite element, and finite volume etc., are used to solve natural convection problems. From last two decades, a new numerical method called lattice Boltzmann method has also been used to simulate wide variety of natural convection problems [3-5].

Lattice Boltzmann method in conjunction with single relaxation [6] collision operator (LBGK) is widely used to simulate dynamics of mesoscopic fluid flow system through fictitious particles collision and normalization to equilibrium state. Under a low Mach number assumption, Chapman-Enskog analysis [7] of LB equation associates moments of equilibrium particles to physical (macroscopic) fluid flow variables, such as density, velocity, temperature, etc., in Navier-Stokes equations. Actually, LBGK simulates nearly incompressible Navier-Stokes equations. In order to account for inherent compressibility

effect, couple of incompressible LBGK models are proposed [8-10]. In addition, a recent study [11] showed that Chapman-Enskog analysis of LBGK cannot recover Navier-Stokes equations precisely and regularization of particle distribution functions in LBGK leads to exact Navier-Stokes equations.

Also, LBGK method is applied successfully to simulate heat transfer in incompressible fluid flows. In thermal incompressible flow, temperature can be treated as a passive scalar that is advected by the flow field [12]. Various thermal LBGK models [12-15] are proposed that are simple and stable for simulation of passive temperature field. In these models, an independent energy density distribution function is used to simulate temperature field. Several researchers have used passive scalar LBGK models to study heat convection [3-5].

Concurrently, during last two decades, several types of fluid flow [16-19] and thermal [4, 20-22] boundary conditions were proposed. Among them, velocity and pressure boundary conditions proposed by Zou and He (1997) [16], and temperature boundary condition proposed by Guo et al., (2002) [22], are widely applied. However, recent regularized fluid flow boundary condition presented by Latt et al., (2008) [18], is found to increase the stability and accuracy of the simulations and thermal boundary condition by Huang et al., (2011) [21], is found to perform better.

It can be noticed from the literature that the most of single-phase thermal flow studies have applied or tested thermal LBGK model to simulate natural convection in enclosures [12, 21], cavities [3, 5, 13-15, 21], cavity with moving lid [13, 20] and annulus space [5, 21] at large. However, to the best of authors' knowledge, the authors natural convection in channels involving pressure inlet and pressure outlet boundary condition simultaneously is not investigated using LBGK, which has numerous applications in electronic cooling [1, 2]. More importantly, RLBGK is a recently proposed method and it has not been used (or sparingly used) to simulate heat convection problems. Therefore the aim of this paper is to study incompressible laminar natural convection in vertical and inclined 2D channels using incompressible RLBGK and passive scalar thermal LBGK method for wide range of Rayleigh numbers, in conjunction with recently proposed fluid flow [18] and thermal [21] boundary conditions.

2.0 METHODOLOGY

2.1 Lattice BGK Equation for Flow Field

Incompressible LBGK model proposed by [8] is adopted here. In LBM, space is discretized into uniform lattice size of δx and velocity is discretized into finite number of velocities $\vec{C}_i$ to form particle distribution functions $f_i(\vec{r},t)$. The LBGK evolution equation is as follows.

$$f\left(\vec{r}+\delta t\vec{c}_i,t+\delta t\right)-f\left(\vec{r},t\right)=-\Omega_i+FT_i,\ \ \Omega_i=\omega\left(f_i-f_i^{eq}\right) \tag{1}$$

Ω_i is the BGK collision operator which defines particle interaction on a lattice sites. FT_i represents body force. Flow dynamics evolve through series of collision and streaming of particle distribution functions. During each time step before collision, particle distribution functions are regularized following the method in ref [11]. Macroscopic variables of the flow are recovered by the moments of particle distribution functions and are as follows.

Penerbit Akademia Baru
Journal of Advanced Research in Fluid Mechanics and Thermal Sciences
ISSN (online): 2289-7879 | Vol. 10, No. 1. Pages 11-26, 2015

$$\rho = \sum_i f_i^{eq}, \quad \rho_0 u_\alpha = \sum_i c_{i\alpha} f_i^{eq} + \delta t \frac{\vec{F}_i}{2} \text{ , and } \Pi_{\alpha\gamma} = \sum_i c_{i\alpha} c_{i\gamma} f_i \tag{2}$$

Equilibrium distribution function is obtained by expansion of Maxwell-Boltzmann equation to second order and it reads as follows.

$$f_i^{eq} = w_i \left[\rho + \rho_0 \left(\frac{1}{c_s^2} \vec{c}_i . \vec{u} + \frac{1}{2c_s^2} Q_i : \vec{u}\vec{u} \right) \right] \tag{3}$$

In Eq. (3), "." is a dot product between two vectors, and ":" refers to contraction between two tensors. Tensors Q are defined as $Q_{\alpha\gamma i} = \vec{c}_{\alpha i} \vec{c}_{\gamma i} - c_s l$, where l is identity, c_s is speed of sound, and $\vec{c}_i$, and t_i are lattice vectors and weights, respectively. Non-equilibrium stress tensors are needed during evolution and are calculated as in Eq. 4.

$$\Pi_{\alpha\gamma}^{neq} = \Pi_{\alpha\gamma} - \Pi_{\alpha\gamma}^{eq} \tag{4}$$

The D2Q9 lattice model is used in the study in which i varies from 1 to 9 and corresponding lattice vector and weights are presented in Eq. 5.

$$\vec{c}_i = \begin{vmatrix} 0 & 1 & 0 & -1 & 0 & +1 & -1 & -1 & +1 \\ 0 & 0 & 1 & 0 & -1 & +1 & +1 & -1 & -1 \end{vmatrix}, \text{ and } t_i = \left[\frac{4}{9}, \frac{1}{9}, \frac{1}{9}, \frac{1}{9}, \frac{1}{9}, \frac{1}{36}, \frac{1}{36}, \frac{1}{36}, \frac{1}{36} \right] \tag{5}$$

Link between moments of particle distribution functions and macroscopic fluid flow variables can be established through a multi-scale Chapman-Enskog analysis [7] of Eq. 1, in which zeroth order term of particle distribution function are equal to equilibrium distribution function $\left(f_i^0 = f_i^{eq} \right)$ and first order term of particle distribution function through regularization $\left(f_i^1 \approx f_i^{neq} = \frac{t_i}{2c_s^2} Q_{i\alpha\gamma} \Pi_{\alpha\gamma}^{neq} + \frac{t_i}{4c_s^2} Q_{i\alpha\gamma} \left(\vec{F}\vec{u} + \vec{u}\vec{F} \right) \right)$ is related to momentum flux tensor at low Mach number [11]. Regularization of particle distribution function not only ensures exact recovery of Navier-Stokes equations but also found to enhance stability and accuracy of the LBM simulation through correct representation of boundary conditions [18].

In system of lattice units, the time step δt and lattice space δx are unity. Lattice velocity, Mach number and pressure of the flow are related to lattice variable as in Eq. 6.

$$u = \frac{\delta t}{\delta x}, \quad M = \frac{u}{c_s^2}, \text{and } P = \rho c_s^2 \tag{6}$$

In Eq. 1, ω is the inverse single relaxation time of particle distribution function. From Champan-Enskog expansion kinematic viscosity of the fluid is related to inverse relaxation time of particle distribution function as follows:

$$\nu = c_s^2 \left(\frac{1}{\omega} - \frac{1}{2} \right) \tag{7}$$

Penerbit Akademia Baru
Journal of Advanced Research in Fluid Mechanics and Thermal Sciences
ISSN (online): 2289-7879 | Vol. 10, No. 1. Pages 11-26, 2015

In LBGK simulation, Kinematic viscosity Eq. 7 is the key variable that is related to Reynolds, Ra, and Gr numbers of the macroscopic fluid flow system.

2.2 Lattice BGK Equation for Temperature Field

As mention earlier, for incompressible fluid flow, viscous heat dissipation and compression work carried out by the pressure are negligible [12]. Hence, energy transport equation for incompressible fluid flow is essentially a convective-diffusive equation of temperature. Here passive scalar LBGK is used to simulate temperature field thru energy density distribution functions. Evolution equation for energy density distribution is as follows.

$$g_i\left(\vec{r}+\delta t\vec{e}_i, t+\delta t\right)-g_i\left(\vec{r},t\right)=-\omega_t\left(g_i-g_i^{eq}\right) \tag{8}$$

ω_t in Eq. 8 is inverse relaxation time of energy density distribution function. Macroscopic temperature is recovered by the moment of energy density distribution functions as in Eq. 9.

$$T=\sum\nolimits_i g_i^{eq} \tag{9}$$

Again, equilibrium energy density distribution function is obtained by expansion of Maxwell-Boltzmann equation. Terms up to first order are sufficient to recover convective-diffusion equation of temperature, and it is as follows.

$$g^{eq}=z_i\left(1+\frac{1}{c_s^2}\vec{e}_i.\vec{u}\right) \tag{10}$$

In Eq. 10, where $\vec{e}_i$ and z_i are lattice vectors and lattice weights, respectively. The D2Q5 lattice model is used in the study in which i varies from 1 to 5 and corresponding lattice vectors, $\vec{e}_i$ and weights, z_i are presented in Eq. 11.

$$\vec{e}_i=\begin{vmatrix}0&1&0&-1&0\\0&0&1&0&-1\end{vmatrix},\ z_i=\left[\frac{4}{3},\frac{1}{3},\frac{1}{3},\frac{1}{3},\frac{1}{3}\right] \tag{11}$$

Again, from Champan-Enskog analysis [7] of Eq. 8, thermal diffusivity λ_d and inverse relaxation time of energy density distribution function is related as in Eq. 12.

$$\lambda_d=c_s^2\left(\frac{1}{\omega_t}-\frac{1}{2}\right) \tag{12}$$

Boussinesq approximation is used in the study, which assumes that all fluid properties, such as density, viscosity, thermal diffusivity are constants for calculating flow dynamics except in the body force term. Body force represents effect of temperature on flow dynamics. The coupling between the temperature and the flow field is achieved by adding a body force term as in equation Eq. 1. Force term recommended by [22] is used and it reads as in Eq. 13.

$$FT_i=\left(1-\frac{\omega}{2}\right)w_i\left(\frac{\left(\vec{c}_i-\vec{u}\right)}{c_s^2}+\frac{\left(\vec{c}_i-\vec{u}\right)}{c_s^4}\vec{c}_i\right).\vec{F}_i \tag{13}$$

Penerbit Akademia Baru

Journal of Advanced Research in Fluid Mechanics and Thermal Sciences
ISSN (online): 2289-7879 | Vol. 10, No. 1. Pages 11-26, 2015

where $\vec{F}$ is the buoyancy force given as $\rho_{ref}\vec{g}\beta\left[T-T_{ref}\right]$.

3.0 BOUNDARY CONDITIONS

3.1 Velocity

Fig. 1 shows the schematics of computational domain with corresponding orientation of particle distribution functions at the boundaries. At the outlet zero gauge pressure is assigned by setting mean density ρ_0 to 1. Unlike in forced or mixed convection, velocity at the inlet is not known priori. Moreover, in LBGK simulations velocity and pressure (density) are implicitly coupled. Usually in conventional numerical methods [23], Bernoulli's equation is used to calculate unknown pressure. In line with conventional numerical methods, pressure at the inlet is calculated from the evolving velocity field iteratively based on Bernoulli's equation and it reads as $\rho_{in}=\rho_0-\frac{3}{2}\rho_0 u_{in}^2$, and $u_{in}=\rho_{in}-\sum_{1,3,5}f_{in}-2\sum_{4,7,8}f_{in}$. As mentioned earlier, LBM simulation involving pressure inlet boundary condition is unaddressed before. Set of distribution functions introduced here in this paper is for the first time. For all cases, no-slip velocity condition is assigned at walls. These macroscopic boundary conditions are casted into regularized particle distribution functions following the procedure of [18]. In which, concept of bounce back of non-equilibrium distribution function [16] is used to construct all unknown particle distribution functions at the boundaries and then non-equilibrium stress tensor components are calculated. These stress tensor components along with equilibrium particle distribution functions are inversed to from regularized particle distribution functions at the boundaries. For the sake of brevity, expressions of unknown non-equilibrium stress tensor at the inlet and inlet-top-corner (see Fig. 1) are presented only.

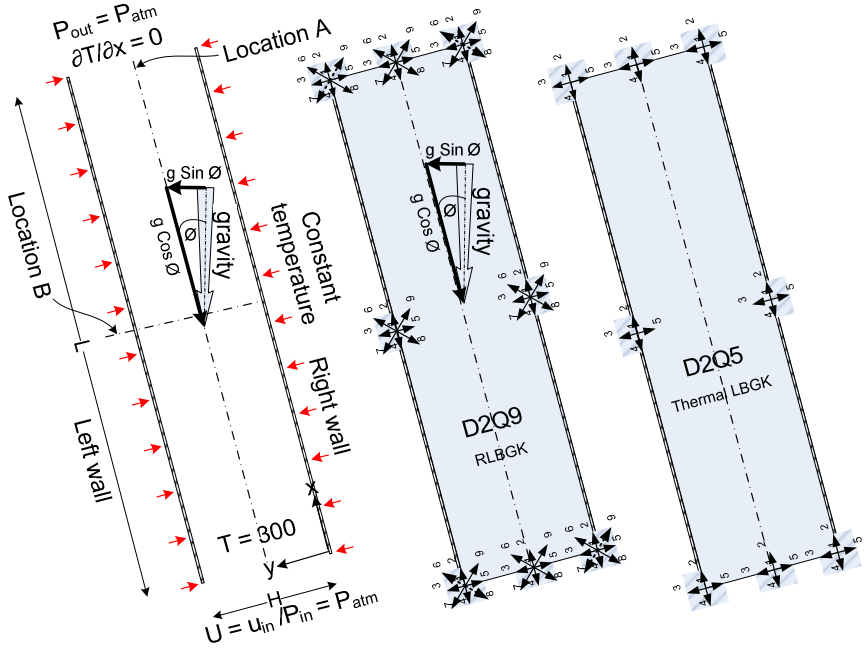

Figure 1: Schematic of inclined channel

Penerbit Akademia Baru
Journal of Advanced Research in Fluid Mechanics and Thermal Sciences
ISSN (online): 2289-7879 | Vol. 10, No. 1. Pages 11-26, 2015

All unknown distribution functions at the boundaries are calculated as following [16]. $f_i^{neq} = f_{(j)}^{neq}$, where j is in opposite direction of i. At the inlet, stress tensors are as follows ($\alpha = x,$ and $\gamma = y$)

$$\Pi_{xx}^{neq} = 2(f_4 + f_7 + f_8) + \rho_0 u_x - \frac{1}{3}\rho - \rho_0 u_x u_x$$
$$\Pi_{yy}^{neq} = 2(f_7 + f_8) + f_3 + f_5 + \rho_0 u_x - \frac{1}{3}\rho_0 u_x - \frac{1}{3}\rho - \rho_0 u_y u_y$$
$$\Pi_{yx}^{neq} = \Pi_{xy,i}^{neq} = 2(f_7 + f_8) - \rho_0 u_x u_y + \frac{1}{3}\rho_0 u_y$$

Similar expressions are obtained for outlet and walls.

At the inlet-top-corner, second order extrapolation scheme is used to estimate the density, and unknown particle distribution function is

$$f_6 = \frac{1}{2}\left(\rho - f_1 - 2(f_7 + f_3 + f_4) - \frac{2}{3}\rho_0 u_x + \rho_0 u_y\right)$$

Stress tensors are as follows

$$\Pi_{xx}^{neq} = 2(f_4 + f_7 + f_6) - \frac{1}{3}\rho + \frac{2}{3}\rho_0 u_x - \frac{1}{3}\rho_0 u_y - \rho_0 u_x u_x$$
$$\Pi_{yy}^{neq} = 2(f_3 + f_7 + f_6) - \frac{1}{3}\rho - \rho_0 u_y - \rho_0 u_y u_y$$
$$\Pi_{xy}^{neq} = 2(f_7 + f_6) - \frac{1}{3}\rho_0 u_x - \rho_0 u_x u_y$$

Similar expressions are obtained for other corners.

3.2 Temperature

For all cases, at the inlet uniform temperature profile is assigned. Temperature at the outlet is extrapolated from neighboring nodes using second order scheme. While at walls, temperature is set to a constant value to match the required Rayleigh number. These macroscopic boundary conditions are translated into regularized energy density distribution functions following the procedure of Haung et al., (2011) [21]. Again, for the sake of brevity, expressions of unknown energy density distribution functions at the inlet and inlet-top-corner (see Fig. 1) are presented only. At the inlet ($\alpha = x,$ and $\gamma = y$).

$g_2 = g_2^{eq} - 0.5 e_{xi}\sigma_x$, where $\sigma_x = \sum_i e_{xi} g_i - T u_{x\_at\_inlet}$

Similar expressions are obtained for outlet and walls. At the corners, second order extrapolation scheme is used to estimate the density and unknown particle distribution function is:

$g_2 = g_2^{eq} - 0.5 e_{xi}\sigma_x$, where $\sigma_x = \sum_i e_{xi} g_i - T_{inlet} u_{x\_inlet}$

Penerbit Akademia Baru
Journal of Advanced Research in Fluid Mechanics and Thermal Sciences
ISSN (online): 2289-7879 | Vol. 10, No. 1. Pages 11-26, 2015

$g_5 = g_5^{eq} - 0.5 e_{yi} \sigma_y$, where $\sigma_y = \sum_i e_{yi} g_i - T_{inlet} u_{y\_inlet}$

Similar expressions are obtained for other corners.

4.0 RESULTS AND DISCUSSION

Schematic of inclined channel is shown in Fig. 1. Channel height and inlet temperature are chosen as reference length and temperature, respectively. Velocity and temperature are normalized as in ref [1] and Nusselt number is based on inlet temperature. Angle of inclination 'Ø' is the angle between the channel axis and the gravity vector. Three inclination angles 0, 30 and 60 ° are considered in the study. Aspect ratio (channel length to height) of the channel is chosen as five. MATLAB software was used for coding. All simulations were carried out on HP desktop with Intel Core i3 processor and 4GB of RAM.

Present simulations consider air as the working fluid. The values of air properties are as follows: density, $\rho_{ref=1.225}$ *kg/m*^{3}, dynamic viscosity, $\mu = 1.94^{-5}$ *kg/m-s,* thermal conductivity, k = 0.0275 *W/m-K* and specific heat capacity, C_p= 1006 *j/kg-K*. Prandlt number $\mu C_p / k$ is 0.71. Rayleigh number $\left(g\beta\left(T - T_{ref}\right)H^3 / \upsilon^2\right)$, *Ra* is varied from 10^2 to 10^6.

For validation of results from the present code, finite volume code Fluent [23], is used for simulation of equivalent macroscopic natural convection in channels. Results are compared at the end of this section.

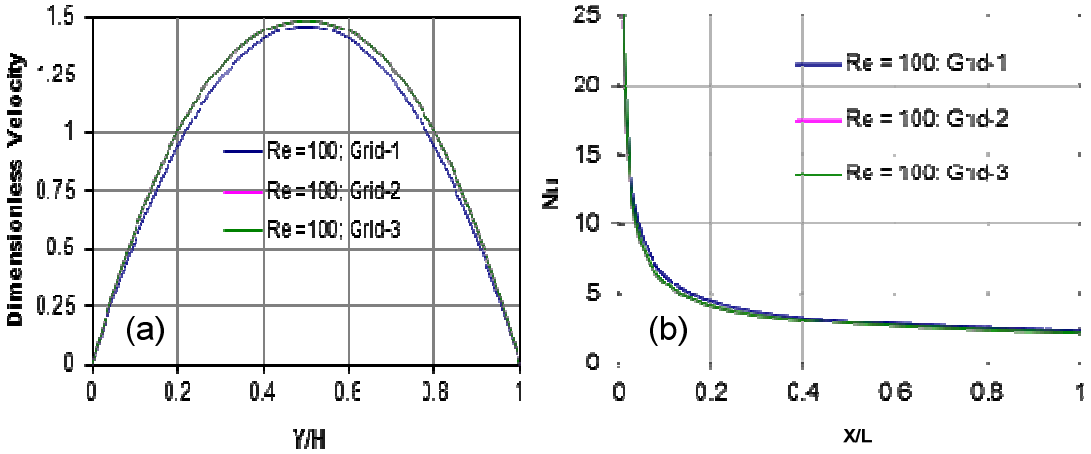

Figure 2: Grid dependency test: (a) Velocity, (b) Nusselt number.

For grid dependency test, laminar force convection in a channel is considered. Reynolds number is set to 100. Three grids are considered namely, grid-1 (81 × 401), grid-2 (101 × 501) and grid-3 (121 × 601). Fig. 2a and 2b show the velocity and Nusselt number obtained from different grids, respectively. Comparison of velocity and Nusselt number from different grids reveals that grid-2 resolution is sufficient for obtaining accurate results. Grid-2 is used for all simulations except for Rayleigh number of 10^6, where grid with 121 × 601 lattice nodes is used. In present simulations relaxation time, τ is set to 0.7. For simulation with

Journal of Advanced Research in Fluid Mechanics and Thermal Sciences
ISSN (online): 2289-7879 | Vol. 10, No. 1. Pages 11-26, 2015

fluent code a non-uniform grid with 60×150 nodes is used. Table 1 shows details of simulation cases considered in the present study. For all simulations initial velocity and temperature are set to zero. Velocity and temperature field of forced convection in a channel is used as reference for comparison.

Table 1: Simulation cases

Rayleigh No.	Case No.	Inclination angle (Ø)
100	1	0°
	2	30°
	3	60°
1000	4	0°
	5	30°
	6	60°
10000	7	0°
	8	30°
	9	60°
50000	10	0°
	11	30°
	12	60°
100000	13	0°
	14	30°
	15	60°

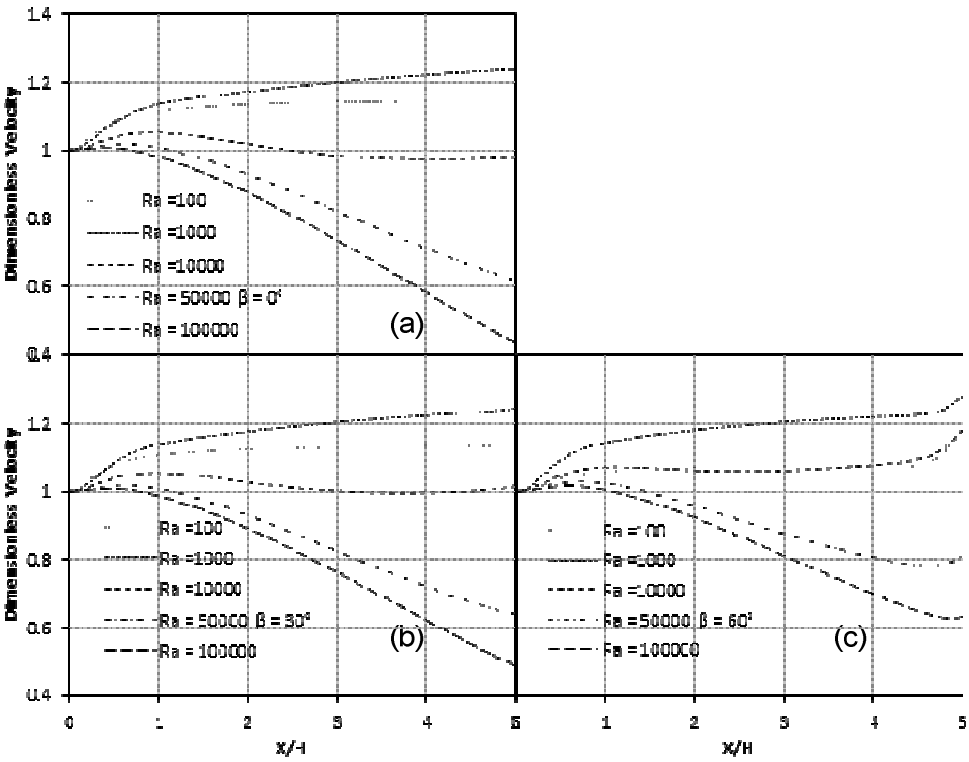

Figure 3: Normalized velocity for various Raleigh numbers at location-A. (a) Ø = 0 °, (b) Ø = 30°, and (c) Ø = 60°.

Penerbit Akademia Baru
Journal of Advanced Research in Fluid Mechanics and Thermal Sciences
ISSN (online): 2289-7879 | Vol. 10, No. 1. Pages 11-26, 2015

Fig. 3 shows the normalized velocity for various Rayleigh number in vertical and inclined channel at location-A (see Fig. 1). For various Rayleigh number, Fig. 3a shows normalized velocity profiles for vertical channel (Ø = 0°), while Fig. 3b and 3c show normalized velocity profiles for inclined channels with inclination angle of 30 and 60°, respectively. In Fig. 3a, for forced convection, velocity increases along the channel to reach a fully developed state at the outlet. Magnitude of velocity decreases asymptotically with increase in Rayleigh number (up to Ra = 10^4). This is because higher buoyancy force acting in the near wall region pulls the fluid towards the outlet, while fluid in the core region is pushed towards the inlet to conserve the momentum. Further increase in Rayleigh number decreases the magnitude of the velocity drastically, especially in the downstream region of the channel, showing the pronounced effect of buoyancy force. For inclined channels, similar behavior of velocity field for various Rayleigh number is observed that can be noticed in Fig. 3b and Fig. 3c. For 60° inclined channel, magnitude of velocities are relative higher when compared with velocity of other cases. This is because buoyancy is acting at an angle towards the left wall that hampers the momentum of the fluid next to the left wall, thus to balance the momentum, fluid at the core and near wall region attain higher velocity.

Fig. 4 shows the normalized velocity for various Rayleigh number in vertical and inclined channels at location-B (see Fig. 1). For forced convection velocity profile is parabolic. When Rayleigh number is increased to 10^3 no appreciable change in velocity profile is observed. Further increase in Rayleigh number increases the buoyancy force in the near wall region that pulls the fluid towards the outlet, while buoyancy force in the core region pushes the fluid towards the inlet that can be observed in Fig. 4a. This phenomenon is more pronounced at higher Rayleigh number. For inclined channels, in Fig. 4b and 4c, similar behavior of velocity field for various Rayleigh number is observed with an exception that velocity field is asymmetric. This is because buoyancy force is acting at an angle. For 60° inclined channel, magnitude of velocities are relative lower when compared with velocity of other cases.

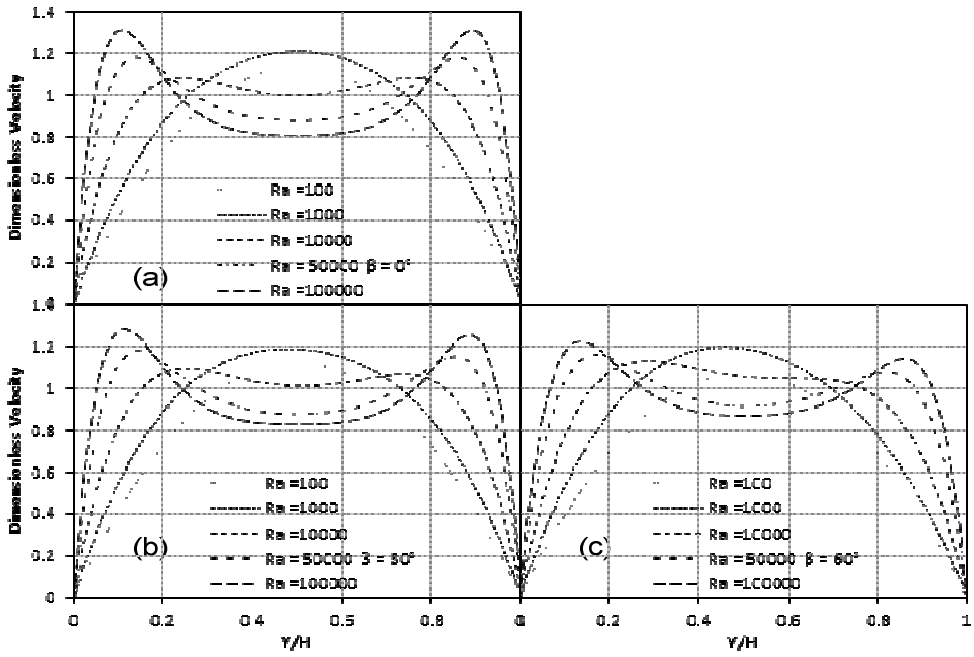

Figure 4: Normalized velocity for various Raleigh numbers at location-B. (a) Ø = 0°, (b) Ø = 30°, and (c) Ø = 60°.

Penerbit Akademia Baru
Journal of Advanced Research in Fluid Mechanics and Thermal Sciences
ISSN (online): 2289-7879 | Vol. 10, No. 1. Pages 11-26, 2015

Fig. 5 shows the normalized temperature for various Rayleigh number in vertical and inclined channels at location-A (see Fig. 1). For forced convection, temperature increases linearly at downstream region of the channel. Also, for moderate range of Rayleigh number (up to Ra = 10^4), temperature increases linearly at downstream region of the channel. For higher Rayleigh numbers, temperature increase asymptotically and exponentially at downstream region of the channel that can be observed in Fig. 5a. For inclined channels, in Fig. 5b and 5c, similar behavior of temperature fields is observed, except that drastic increase in temperature is observed close to outlet for 60° inclined channel for high Rayleigh number. This is due to occurrence of flow reversal in the region.

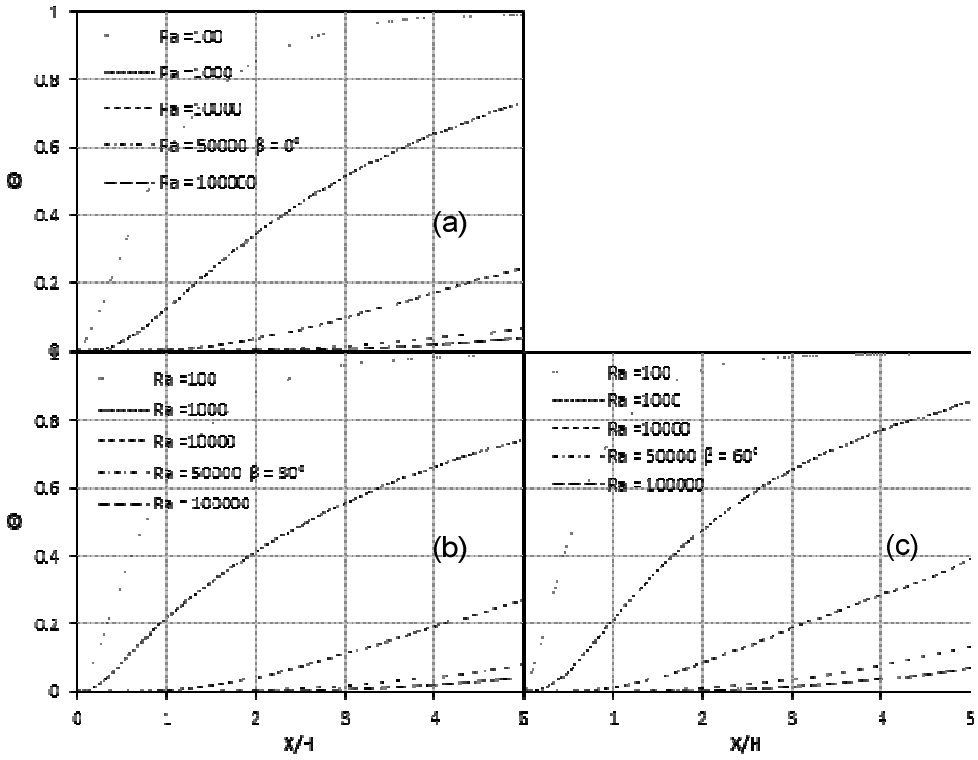

Figure 5: Normalized temperature for various Raleigh numbers at location-A. (a) Ø = 0 °, (b) Ø = 30°, and (c) Ø = 60°.

Fig. 6 shows the normalized temperature for various Rayleigh number in vertical and inclined channels at location-B (see Fig. 1). For forced convection, the temperature profile is a inverse parabola. Temperature is high at near wall regions and low at core region of the channel. At the near wall region of the channel, temperature profile gets steeper with increase in Rayleigh number, while at the core region of the channel, temperature profile remain constant except for high Rayleigh number that can be observed in Fig. 6a. Increase in temperature in core region of the channel at high Rayleigh number reveals fluid entrainment in the region. For inclined channels, in Fig. 6b and 6c, similar behavior of temperature field can be observed except that temperature profile is relatively steeper at the right wall.

Penerbit Akademia Baru
Journal of Advanced Research in Fluid Mechanics and Thermal Sciences
ISSN (online): 2289-7879 | Vol. 10, No. 1. Pages 11-26, 2015

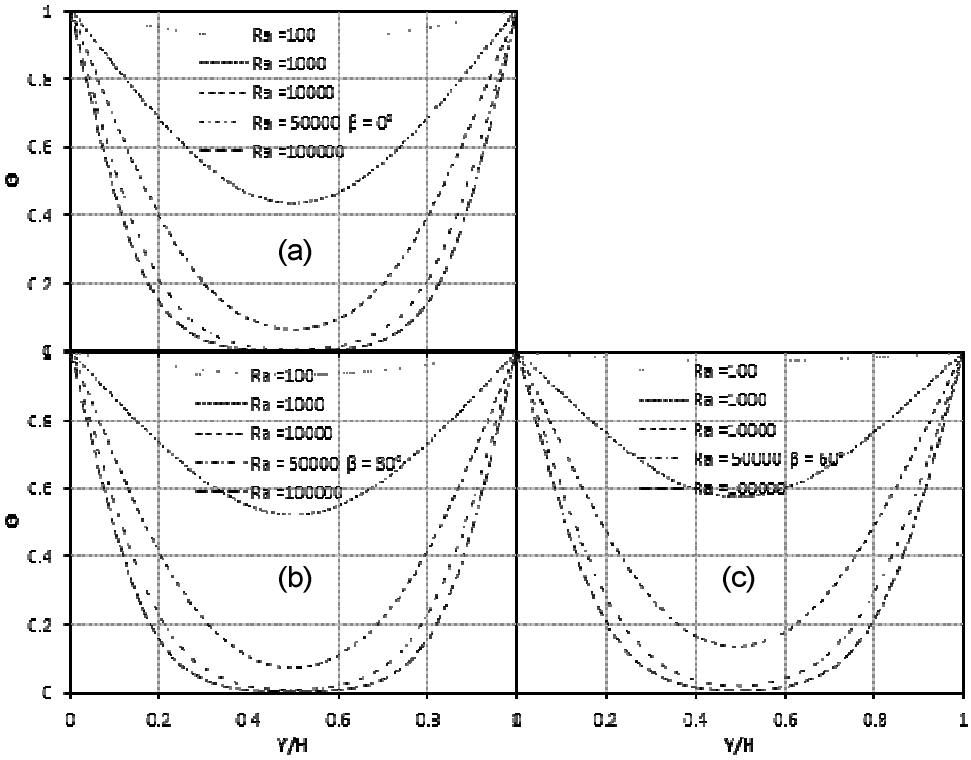

Figure 6: Normalized temperature for various Raleigh numbers at location-B. (a) Ø = 0°, (b) Ø = 30 °, and (c) Ø = 60 °

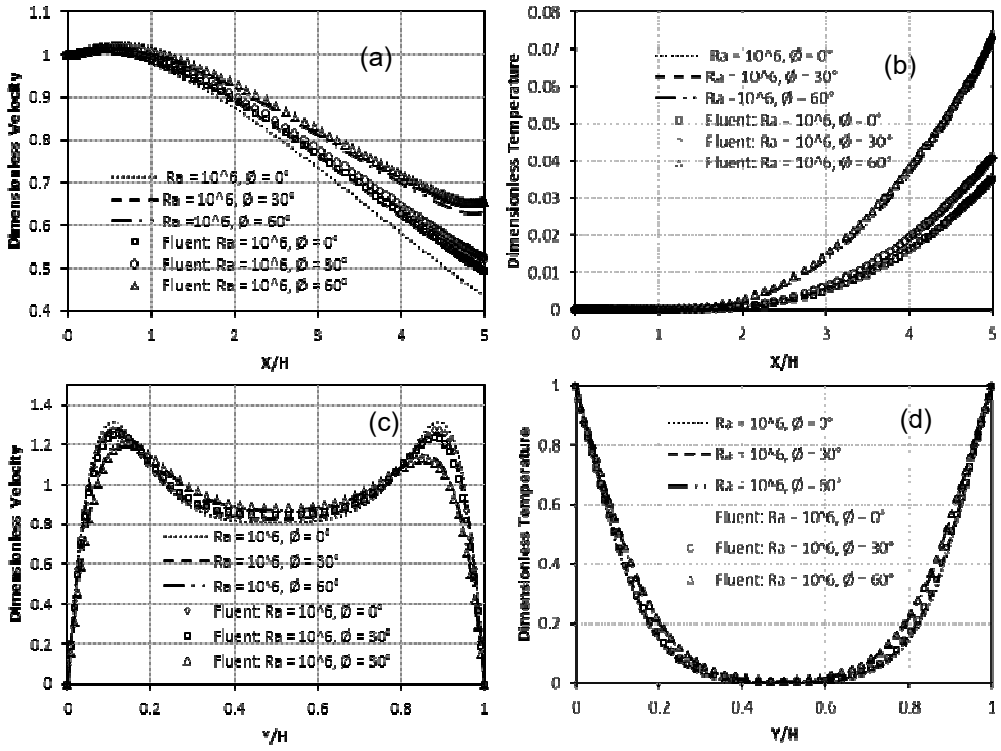

Figure 7: Comparison of normalized velocity and temperature for Ra = 5×104. (a) & (b) location-A, (c) & (d) location-B.

Penerbit Akademia Baru
Journal of Advanced Research in Fluid Mechanics and Thermal Sciences
ISSN (online): 2289-7879 | Vol. 10, No. 1. Pages 11-26, 2015

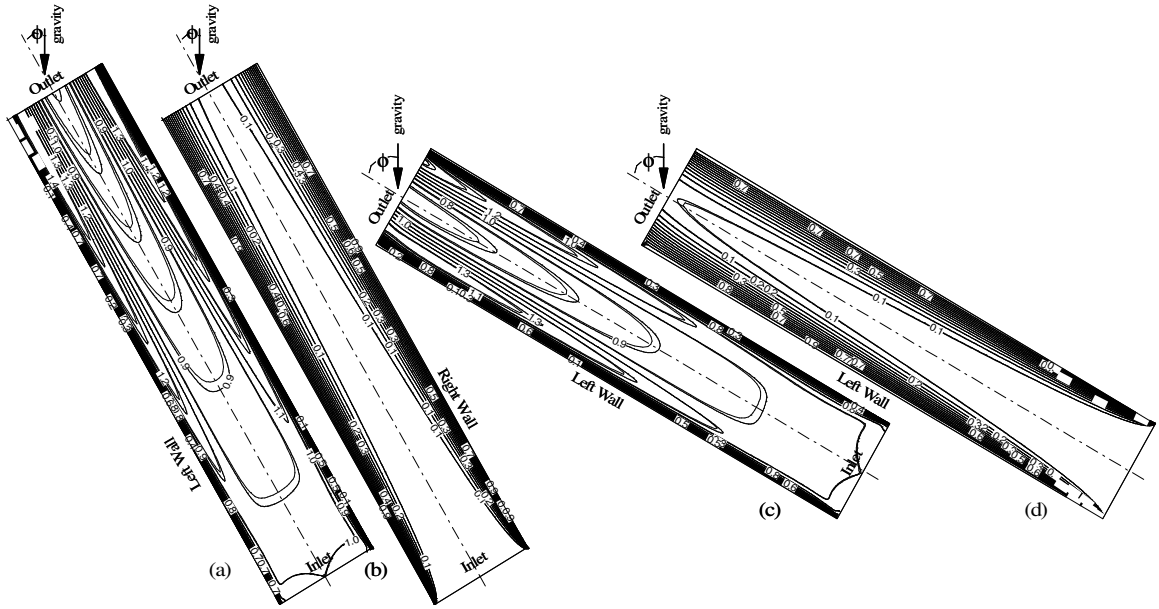

Figure 8: Comparison of normalized velocity and temperature field. Ra = 10^6. (a) β = 30° Velocity, (b) β = 30° Temperature, (c) β = 60° Velocity, (d) β = 60° Temperature. Solid line: Present study, Dotted line: Fluent.

For validation, velocity and temperature profiles are compared with velocity and temperature obtained from Fluent code at location A and B. Rayleigh number of 5×10^4 is picked for validation. Fig. 7 show the validation of normalized velocity and temperature profile at location-A and Location-B. For vertical and 30° inclined channels, it can be seen that predicted velocity and temperature compares very well with results obtained from Fluent code. For 60° channel at location A, a small difference in predicted velocity and velocity obtained from Fluent code can be observed in the core region of the channel. Again, at location A, for vertical channel, noticeable difference in predicted temperature and temperature obtained from Fluent code can be observed at downstream of the channel. For local comparison velocity and temperature of whole channel is presented in Fig. 8 for inclined channels at *Ra* 10^6.

In order to be consistent with literature [1, 2], present study calculates Nusselt number based on inlet temperature. Fig. 9 shows Nusselt number for various Rayleigh number in vertical and inclined channel. For forced convection, Nusselt number is high at channel entrance and decrease gradually to attain a constant value of 7.54 at the channel exit. Again here, Nusselt number of forced convection is used as reference for comparison. For vertical channel, Nusselt number is found to increase with increase in Rayleigh number. This is because, as mentioned earlier, buoyancy force enhances the fluid momentum in near wall regions and hence high temperature gradients in the vicinity of the walls. For inclined channels, Nusselt number of right wall is relatively higher than the Nusselt number of left wall, especially for 60° of inclination, which is due to presence of cold fluid in the vicinity of the right wall region. Also, it can be seen that due to flow reversal at the channel outlet, Nusselt number are high and low at left and right wall, respectively, which can be seen in Fig. 9b and 9c. For all cases, comparison of averaged Nusselt number with correlation [24] is presented in Fig. 10. From Fig. 10 it is apparent that the averaged Nusselt number agrees well with the correlation for higher range of Rayleigh number. For Raleigh number range of 10^3-10^6, the percentage error in Nusselt number was within ± 10 range.

Penerbit Akademia Baru
Journal of Advanced Research in Fluid Mechanics and Thermal Sciences
ISSN (online): 2289-7879 | Vol. 10, No. 1. Pages 11-26, 2015

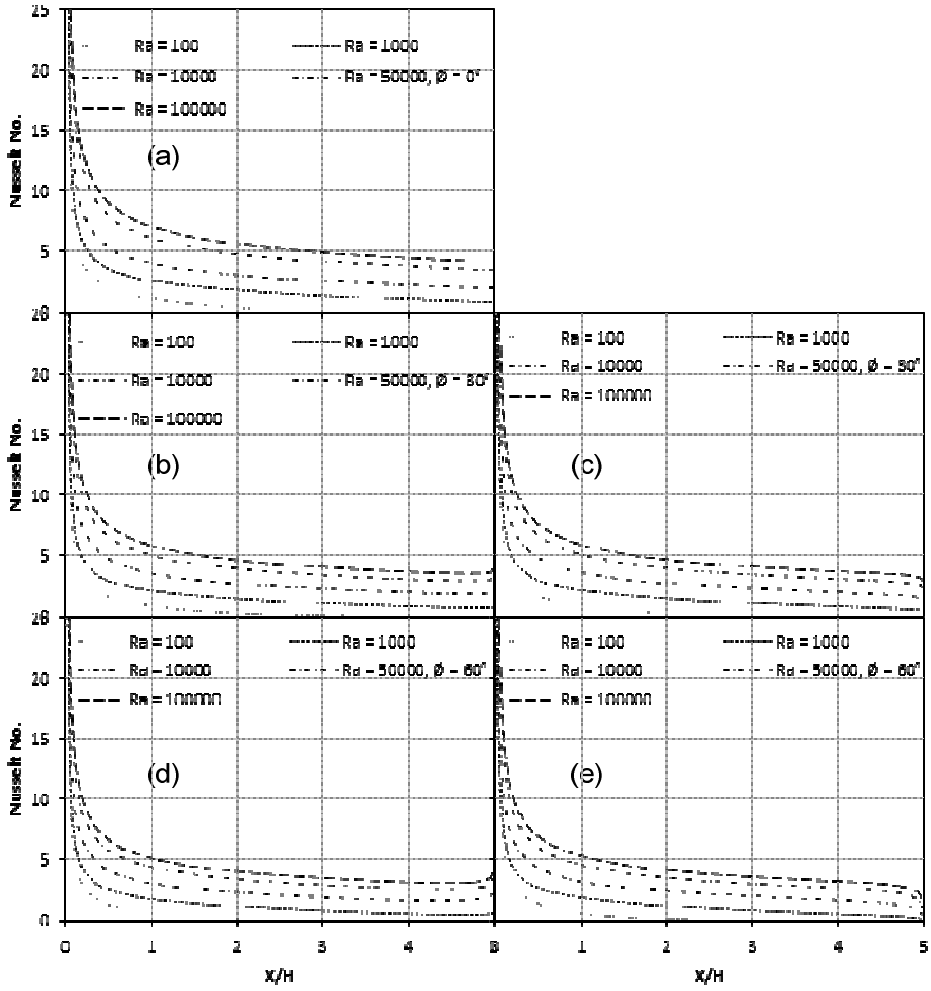

Figure 9: Local Nusselt number along the channel length for various Raleigh numbers. (a) Ø = 0°, (b) Ø = 30° left wall, (c) Ø = 30° right wall, (d) Ø = 60° left wall, and (e) Ø = 60° right wall.

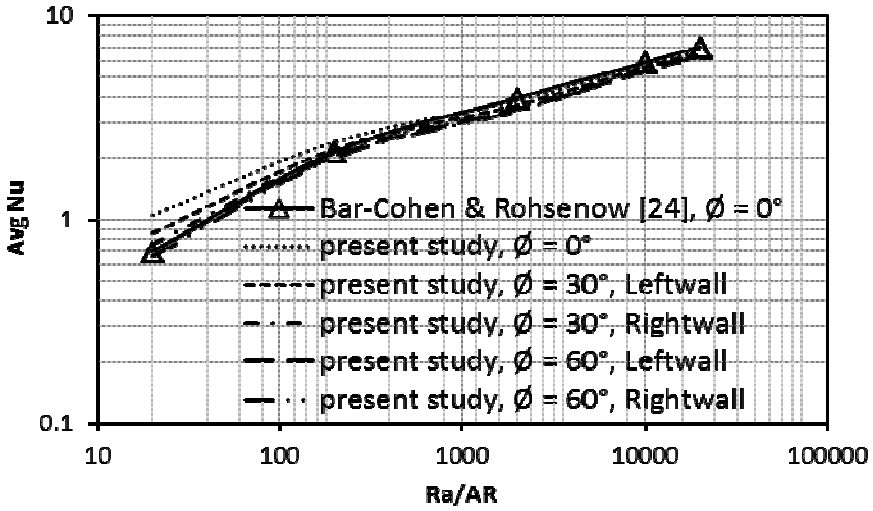

Figure 10: Averaged Nusselt number for various Rayleigh number.

5.0 CONCLUSION

Incompressible laminar natural convection in entrance region of 2D vertical and inclined channels is simulated using RLBGK and thermal LBGK method together with regularized boundary conditions. Rayleigh number is varied from 10^2 to 10^5. The channel orientation is varied from 0 to 60°. Analogous to Bernoulli's equation, equivalent set of distribution functions are proposed to represent pressure at the inlet. Predicted velocity and temperature match with velocity and temperature obtained from Fluent, and averaged Nusselt numbers agree well with correlation of Bar-Cohen and Rohsenow, 1984 [24] for higher range of Rayleigh number. For Raleigh number range of 10^3-10^6, the error in averaged Nusselt number was found to be within ± 10%. The present study concludes that RLBGK in conjunction with passive scalar thermal LBGK is a viable numerical method for simulating natural convection in 2D channels.

NOMENCLATURE

c, e	Micro velocities
f	Density distribution function
f^{eq}	Equilibrium density distribution function
$\vec{F}$	External force, N
g	Internal energy density distribution function
g^{eq}	Equilibrium internal energy density distribution function
Ra	Rayleigh number
t	Time, s
T	Temperature, K
$\vec{u}$	Velocity vector, m/s
β	Thermal expansion coefficient
υ	Viscosity, m^2/s
ρ	Density, kg/m^3
ϕ	Inclination angle
τ	Relaxation time, s
ω	Inverse relaxation time, s
λ	Thermal diffusivity, W/m K
Π	Stress tensor
i	Direction of micro velocity
in	Inlet
α, γ	Indices of direction
eq	Equilibrium
neq	Non-equilibrium

REFERENCE

[1] G. Desrayaud, G. Lauriat, Flow reversal of laminar mixed convection in the entry region of symmetrically heated, vertical plate channels. International Journal of Thermal Sciences 48 (11)(2009) 2036-2045.

[2] X. Wang, D.W. Pepper, Numerical simulation for natural convection in vertical channels. International Journal of Heat and Mass Transfer 52 (17)(2009) 4095-4102.

[3] X. Shan, Simulation of Rayleigh-Bénard convection using a lattice Boltzmann method. Physical Review E 55 (3)(1997) 2780.

[4] S. Chen, Simulating compositional convection in the presence of rotation by lattice Boltzmann model. International Journal of Thermal Sciences 49 (11)(2010) 2093-2107.

[5] C.S. Nor Azwadi, T. Tanahashi, Three-dimensional thermal lattice Boltzmann simulation of natural convection in a cubic cavity. International Journal of Modern Physics B 21 (01)(2007) 87-96.

[6] P.L. Bhatnagar, E.P. Gross, M. Krook, A model for collision processes in gases. I. Small amplitude processes in charged and neutral one-component systems. Physical review 94 (3)(1954) 511.

[7] S. Chapman, T.G. Cowling, The Mathematical Theory of Non-uniform Gases: An Account of the Kinetic Theory of Viscosity, Thermal Conduction and Diffusion of Gases, Notes Added in 1951. 1952: Cambridge university press.

[8] X. He, L.-S. Luo, Lattice Boltzmann model for the incompressible Navier–Stokes equation. Journal of statistical Physics 88 (3-4)(1997) 927-944.

[9] Q. Zou, et al., A improved incompressible lattice Boltzmann model for time-independent flows. Journal of Statistical Physics 81 (1-2)(1995) 35-48.

[10] Z. Guo, B. Shi, N. Wang, Lattice BGK model for incompressible Navier–Stokes equation. Journal of Computational Physics 165 (1)(2000) 288-306.

[11] J. Latt, B. Chopard, Lattice Boltzmann method with regularized pre-collision distribution functions. Mathematics and Computers in Simulation 72 (2)(2006) 165-168.

[12] Y. Peng, C. Shu, Y. Chew, Simplified thermal lattice Boltzmann model for incompressible thermal flows. Physical Review E 68 (2)(2003) 026701.

[13] X. He, S. Chen, G.D. Doolen, A novel thermal model for the lattice Boltzmann method in incompressible limit. Journal of Computational Physics 146 (1)(1998) 282-300.

[14] Z. Guo, C. Zheng, B. Shi, Discrete lattice effects on the forcing term in the lattice Boltzmann method. Physical Review E 65 (4)(2002) 046308.

[15] C.S. Nor Azwadi, T. Tanahashi, Simplified thermal lattice Boltzmann in incompressible limit. International Journal of Modern Physics B 20 (17)(2006) 2437-2449.

[16] Q. Zou, X. He, On pressure and velocity boundary conditions for the lattice Boltzmann BGK model. Physics of Fluids (1994-present) 9 (6)(1997) 1591-1598.

[17] S. Chen, D. Martinez, R. Mei, On boundary conditions in lattice Boltzmann methods. Physics of Fluids (1994-present) 8 (9)(1996) 2527-2536.

[18] J. Latt, et al., Straight velocity boundaries in the lattice Boltzmann method. Physical Review E 77 (5)(2008) 056703.

[19] M. Hecht, J. Harting, Implementation of on-site velocity boundary conditions for D3Q19 lattice Boltzmann. Journal of Statistical Mechanics: Theory and Experiment 13 (2010).

[20] A. D'Orazio, S. Succi, Simulating two-dimensional thermal channel flows by means of a lattice Boltzmann method with new boundary conditions. Future Generation Computer Systems 20 (6)(2004) 935-944.

[21] H. Huang, X. Lu, M. Sukop, Numerical study of lattice Boltzmann methods for a convection–diffusion equation coupled with Navier–Stokes equations. Journal of Physics A: Mathematical and Theoretical 44 (5)(2011) 055001.

[22] Z. Guo, B. Shi, C. Zheng, A coupled lattice BGK model for the Boussinesq equations. International Journal for Numerical Methods in Fluids 39 (4)(2002) 325-342.

[23] A.F. Ansys, 14.0 Theory Guide. ANSYS inc, (2011) 218-221.

[24] A. Bar-Cohen, W. Rohsenow, Thermally optimum spacing of vertical, natural convection cooled, parallel plates. Journal of Heat Transfer 106 (1)(1984) 116-123.